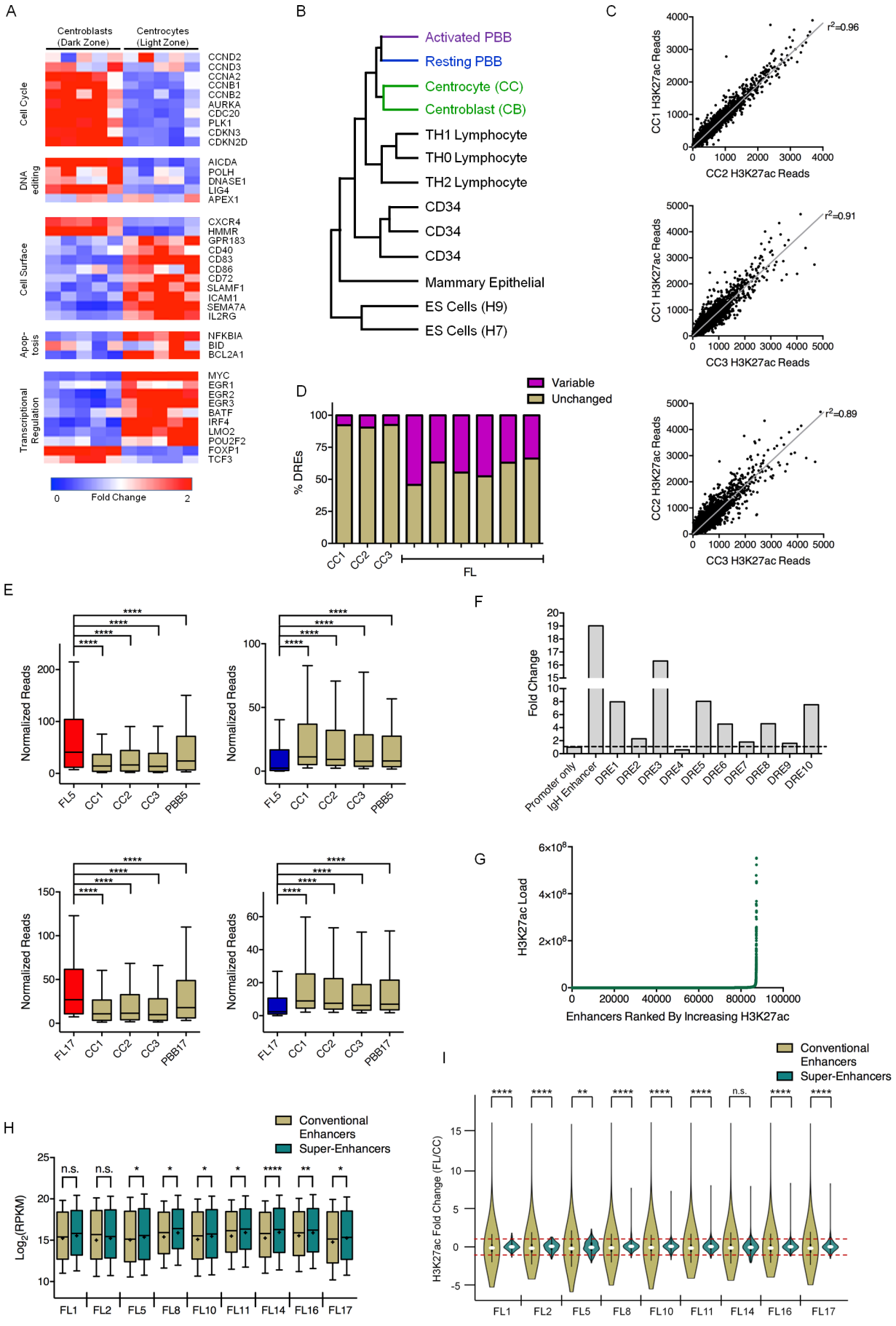
A
Centroblasts (Dark Zone)
Centrocytes (Light Zone)
Cell Cycle
CCND2
CCND3
CCNA2
CCNB1
CCNB2
AURKA
CDC20
PLK1
CDKN3
CDKN2D
DNA editing
AICDA
POLH
DNASE1
LIG4
APEX1
Cell Surface
CXCR4
HMMR
GPR183
CD40
CD83
CD86
CD72
SLAMF1
ICAM1
SEMA7A
IL2RG
Apop-tosis
NFKBIA
BID
BCL2A1
Transcriptional Regulation
MYC
EGR1
EGR2
EGR3
BATF
IRF4
LMO2
POU2F2
FOXP1
TCF3
0
Fold Change
2
B
Activated PBB
Resting PBB
Centrocyte (CC)
Centroblast (CB)
TH1 Lymphocyte
TH0 Lymphocyte
TH2 Lymphocyte
CD34
CD34
CD34
Mammary Epithelial
ES Cells (H9)
ES Cells (H7)
C
CC1 H3K27ac Reads
CC2 H3K27ac Reads
r2=0.96
CC1 H3K27ac Reads
CC3 H3K27ac Reads
r2=0.91
CC2 H3K27ac Reads
CC3 H3K27ac Reads
r2=0.89
D
Variable
Unchanged
% DREs
CC1
CC2
CC3
FL
E
Normalized Reads
FL5
CC1
CC2
CC3
PBB5
FL17
PBB17
F
Fold Change
Promoter only
IgH Enhancer
DRE1
DRE2
DRE3
DRE4
DRE5
DRE6
DRE7
DRE8
DRE9
DRE10
G
H3K27ac Load
Enhancers Ranked By Increasing H3K27ac
H
Conventional Enhancers
Super-Enhancers
Log2(RPKM)
n.s.
FL1
FL2
FL5
FL8
FL10
FL11
FL14
FL16
FL17
I
Conventional Enhancers
Super-Enhancers
H3K27ac Fold Change (FL/CC)
n.s.

Figure S1

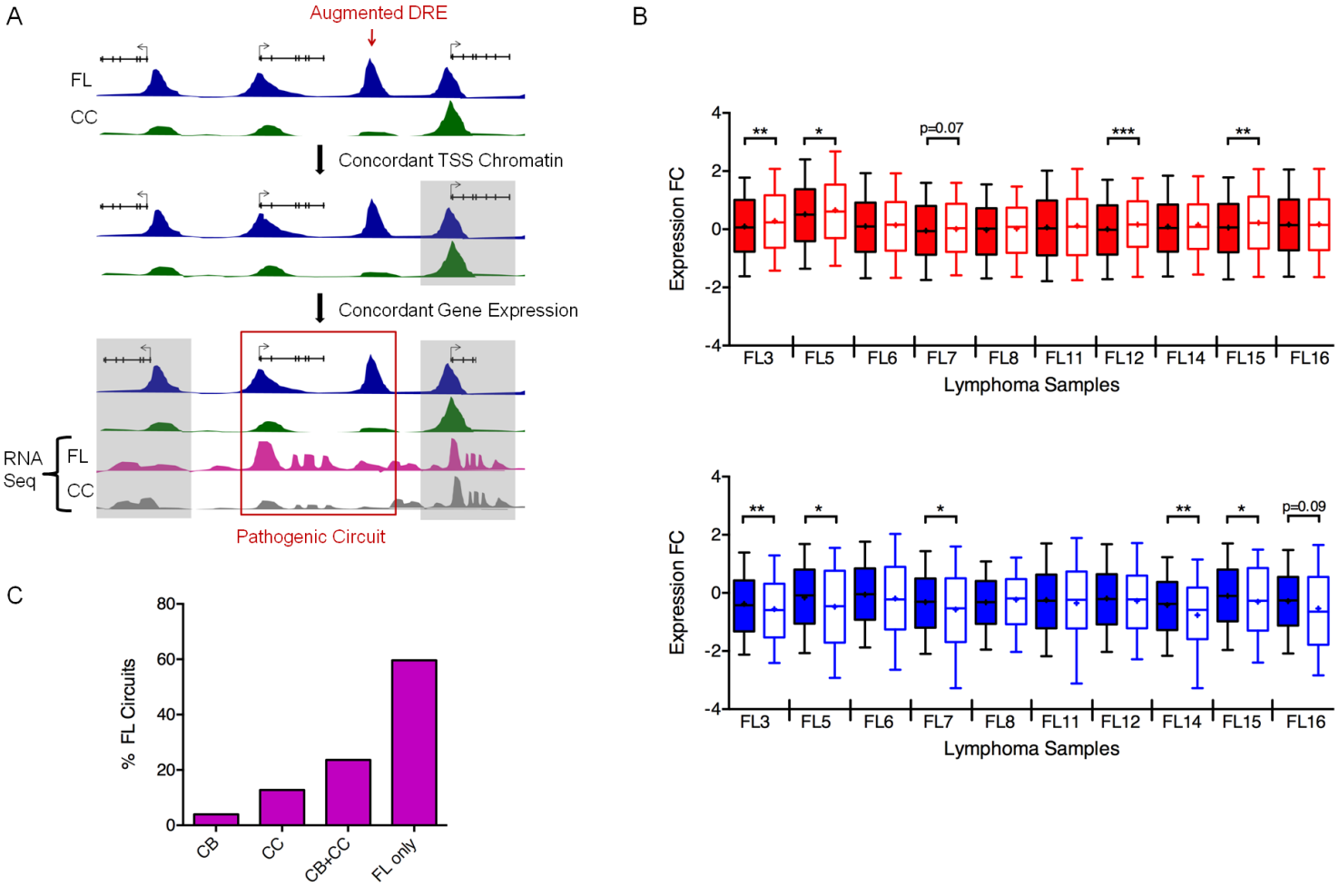
A
Augmented DRE
FL
CC
Concordant TSS Chromatin
Concordant Gene Expression
RNA Seq
FL
CC
Pathogenic Circuit
B
Expression FC
4
2
0
-2
-4
**
*
p=0.07
***
**
FL3
FL5
FL6
FL7
FL8
FL11
FL12
FL14
FL15
FL16
Lymphoma Samples
Expression FC
**
*
*
**
*
p=0.09
Lymphoma Samples
C
% FL Circuits
80
60
40
20
0
CB
CC
CB+CC
FL only

Figure S2

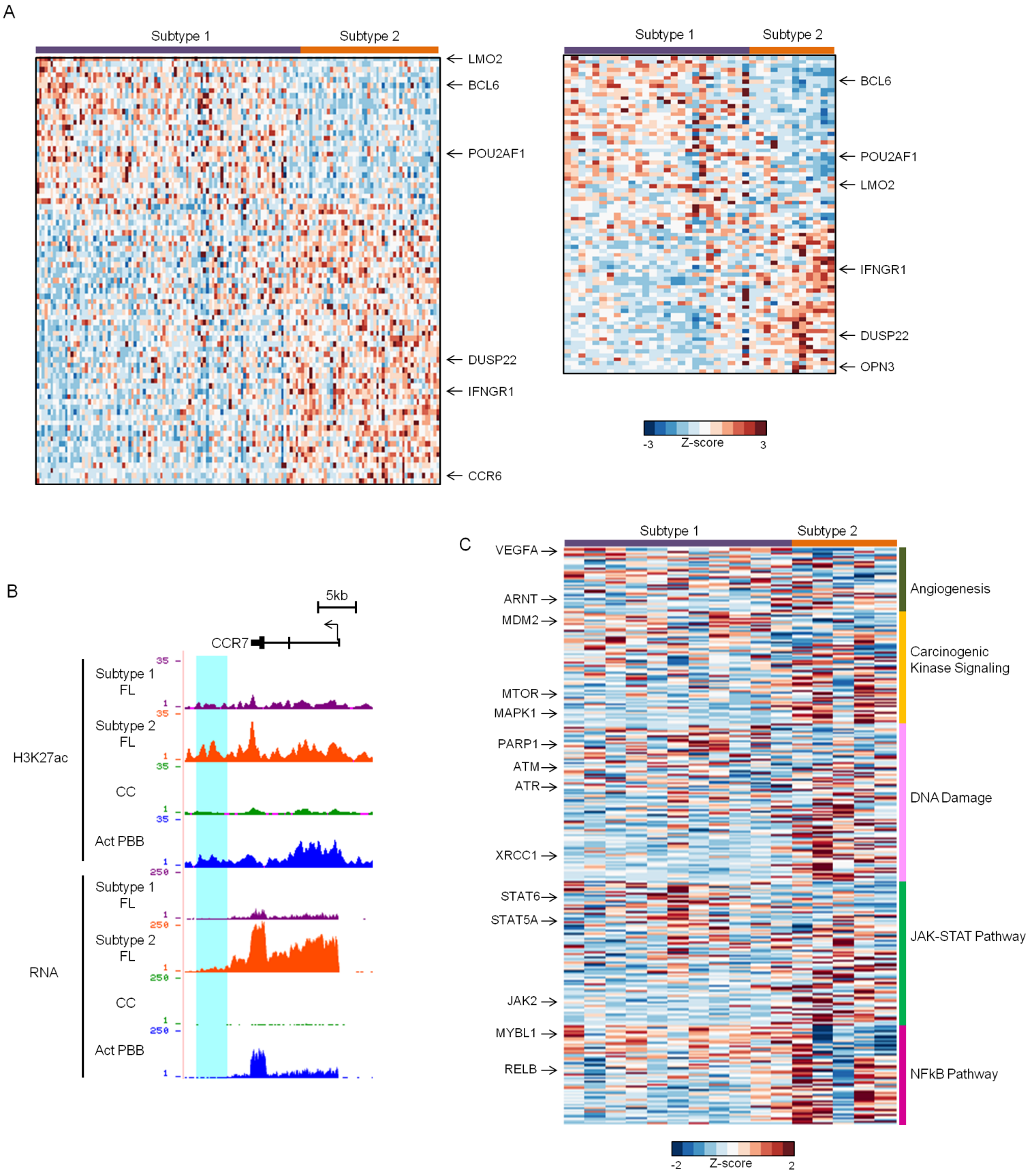
A
Subtype 1
Subtype 2
LMO2
BCL6
POU2AF1
DUSP22
IFNGR1
CCR6
Subtype 1
Subtype 2
BCL6
POU2AF1
LMO2
IFNGR1
DUSP22
OPN3
-3
Z-score
3
B
5kb
CCR7
H3K27ac
Subtype 1 FL
Subtype 2 FL
CC
Act PBB
RNA
Subtype 1 FL
Subtype 2 FL
CC
Act PBB
C
Subtype 1
Subtype 2
VEGFA
ARNT
MDM2
MTOR
MAPK1
PARP1
ATM
ATR
XRCC1
STAT6
STAT5A
JAK2
MYBL1
RELB
Angiogenesis
Carcinogenic Kinase Signaling
DNA Damage
JAK-STAT Pathway
NFkB Pathway
-2
Z-score
2

Figure S3

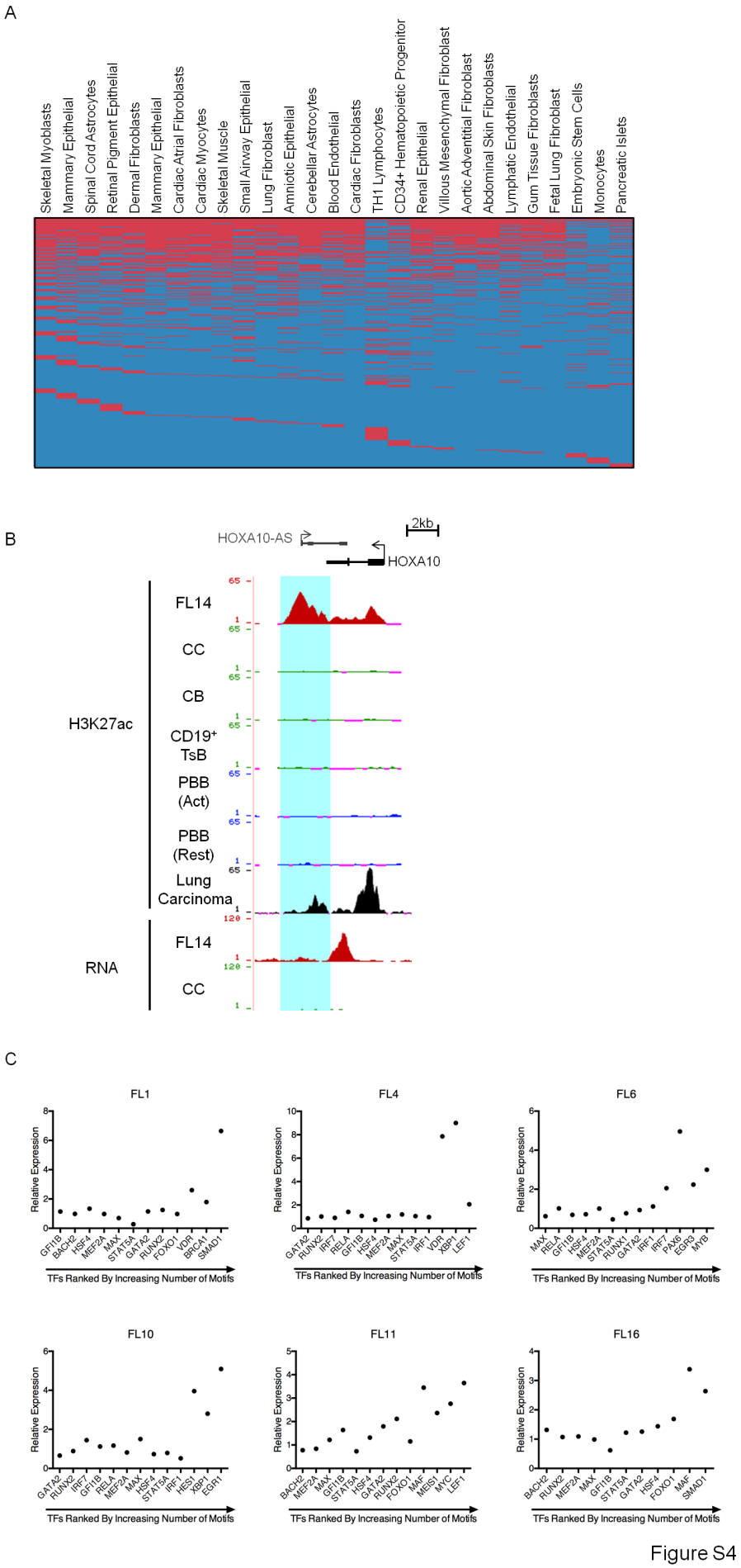
A
Skeletal Myoblasts
Mammary Epithelial
Spinal Cord Astrocytes
Retinal Pigment Epithelial
Dermal Fibroblasts
Mammary Epithelial
Cardiac Atrial Fibroblasts
Cardiac Myocytes
Skeletal Muscle
Small Airway Epithelial
Lung Fibroblast
Amniotic Epithelial
Cerebellar Astrocytes
Blood Endothelial
Cardiac Fibroblasts
TH1 Lymphocytes
CD34+ Hematopoietic Progenitor
Renal Epithelial
Villous Mesenchymal Fibroblast
Aortic Adventitial Fibroblast
Abdominal Skin Fibroblasts
Lymphatic Endothelial
Gum Tissue Fibroblasts
Fetal Lung Fibroblast
Embryonic Stem Cells
Monocytes
Pancreatic Islets
B
HOXA10-AS
2kb
HOXA10
H3K27ac
FL14
CC
CB
CD19+ TsB
PBB (Act)
PBB (Rest)
Lung Carcinoma
RNA
FL14
CC
C
FL1
FL4
FL6
FL10
FL11
FL16
Relative Expression
TFs Ranked By Increasing Number of Motifs

Figure S4

Supplemental Figure Legends

Figure S1, related to Figure 1. Identification of Dyseregulated Enhancers and Superenhancers in FL. A) Expression profiles of germinal center B cell populations for a panel of genes previously shown to distinguish CB and CC cells (Victora et al., 2012). B) Unbiased clustering of open chromatin regions from 10 cell types reveals the close epigenetic relationship between CB and CC (see Experimental Procedures). C) Scatter plots of normalized H3K27ac-Seq data comparing CC samples. D) Bar graph showing percent variable and unchanged DREs when individual CC samples are compared to the average of the other CC samples. For comparison, DRE variability is shown for representative FL samples, calculated compared to the average of all CC samples. Total variable DREs for CC1: 1254, CC2: 1553, CC3: 1230. E) H3K27ac profiles for CC samples and patient-matched PBB. Normalized H3K27ac data show significantly and consistently elevated read densities in augmented (red) and attenuated read densities (blue) in FL5 and FL17 when compared with individual CC samples or to patient-matched PBBs. Statistical significance was determined using Student's *t* test. ****$P < 0.0001$. F) Luciferase reporter assays for ten variable DREs. DRE and IgH enhancer activities were assayed in lymphoma cell lines and are reported relative to a reporter containing only the SV40 promoter. Results are representative of two independent experiments. G) Rank order of increasing H3K27ac enrichment at enhancer loci in a representative FL sample. H) Mean transcript abundance of the genes associated with conventional and super-enhancers in nine FL samples. Statistical significance (Mann-Whitney test): *$p \leq 0.05$ ** $p \leq 0.01$, **** $p \leq 0.0001$. I) Violin plots showing H3K27ac fold change of conventional- and super-enhancers for indicated FL samples. Statistical significance (χ^2 test): ** $p \leq 0.01$, **** $p \leq 0.0001$.

Figure S2, related to Figure 2. Defining Pathogenic Circuits. A) Using a pattern-based strategy, we connected variable DREs to genes located within 500 kb that harbor concordant changes in chromatin at their transcription start sites (TSS). To fully elucidate the pathogenic connections, we also required concordant changes in the expression of putative target genes. Gray boxes represent candidate targets for DREs that were excluded from the circuitry due to a lack of concordance for the respective criteria. B) Expression fold change for all genes located within 500kb of DREs augmented (red) or attenuated (blue) in FL based on analysis of microarray data. Genes with concordant changes in TSS chromatin marks are shown as outlined boxes. Square symbols within each box denote means. Statistical significance (unpaired t-test with Welch's correction): ** $p \leq 0.01$, *** $p \leq 0.001$, **** $p \leq 0.0001$. C) Bar graph depicting the proportions of circuits with perturbed activity in FL that exhibit normal activity levels in GC-B subsets or are unique to FL.

Figure S3, related to Figure 3. FL Subtype 1 and 2 Expression Patterns Differ for Multiple Biological Pathways and in Public Expression Data. A) Expression profiles for the set of TFs that distinguish subtype 1 from subtype 2 FL. Shown are data from two larger sets (GSE12453-left, GSE16131 - right) of unsorted FL biopsies (Dave et al., 2004; Leich et al., 2009). B) UCSC Genome Browser view of H3K27ac ChIP-seq data showing subtype 2-specific DREs (highlighted in blue) downstream of the *CCR7* gene in FL, CC, and *in vitro* activated PBB samples. RNA-seq data depict the corresponding up-regulation of *CCR7* mRNA in subtype 2 FL relative to subtype 1. C) Expression heatmap for FL samples depicting genes in pathways that showed significant differences in subtypes 1 versus 2, as determined by GSEA (FDR $q<0.0001$, see Methods). Several examples of key pathway genes are highlighted to the left of the heatmap.

Figure S4, related to Figure 4. FL Pirates REs from Other Cell Lineages. A) Distribution of 3374 *de novo* REs that overlap regions of open chromatin in at least one of 27 ENCODE non-B cell lineages (coincident, red; non-overlapping, blue) (Bernstein et al., 2012; Thurman et al., 2012). B) UCSC Genome Browser view of H3K27ac ChIP-seq data showing a *de novo* DRE upstream of *HOXA10* that overlaps H3K27ac peaks in lung carcinoma cells (Neph et al., 2012). RNA-seq data depict the corresponding up-regulation of *HOXA10* mRNA in the FL sample relative to CC. C) Relative expression of TFs, ranked by number of corresponding TF motifs within private DREs, in individual FL samples compared to the average of all FL.

Supplemental Tables

Table S1, related to Figure 1. Patient Information

Patient ID	Diagnosis (Grade)	Age	Sex	κ/λ Restriction (% $CD19^+$ cells)	t(14;18)(q32;q21) Translocation	# $CD19^+$ cells purified
FL1	FL3A	44	F	29/69		26 x 10^6
FL 2	FL 1-2	53	M	98/1	MCR PCR	217 x 10^6
FL 3	FL 1	47	F	97/2		62 x 10^6
FL 4	FL 1-2	50	F	99/1		35 x 10^6
FL 5	FL 1-2	52	M	58/42	MBR PCR	98 x 10^6
FL6	FL 1-2	46	F	93/6		7 x 10^6
FL 7	FL 1-2	65	M	71/29		44 x 10^6
FL 8	FL 1	53	F	4/95		88 x 10^6
FL 9	FL 1-2	35	F	6/76	MBR PCR	26 x 10^6
FL 10	FL 1-2	40	M	7/92	MBR PCR	19 x 10^6
FL 11	FL 1-2	78	M	53/35	MBR PCR	91 x 10^6
FL 12	FL 2	57	F	$CD19^+$, κ/λ lost	MBR PCR	114 x 10^6
FL 13	FL 1-2	69	F	7/87	MBR PCR	159 x 10^6
FL 14	FL 1-2	63	F	92/7	MBR PCR	46 x 10^6
FL15	FL 1-2	50	F	90/1	MBR PCR	11 x 10^6
FL 16	FL 1-2	63	F	98/2	FISH/MCR PCR	152 x 10^6
FL 17	FL 1-2	61	M	15/84		4 x 10^6
FL18	FL3A	60	M	97/2	FISH	7 x 10^6

MBR = major breakpoint region
MCR = minor cluster region

Table S2, related to Figure 1. (Provided in .xls format)

Mutations in FL samples.

Table S3, related to Figure 1. (Provided in .xls format)

Super-enhancer genomic locations and their nearest neighbor genes.

Table S4, related to Figure 2. (Provided in .xls format)

Circuits tab: Genomic locations of variable DREs are listed with genes that show concordant chromatin changes at the TSS. DRE coordinates tab: The genomic locations of all numbered DRE shown in Figures 4, 5, 7 and S1. Recurrent DRE tab: The genomic locations of recurrent DREs (≥13 FL) and their putative target genes (located within 100 kb).

Table S5, related to Figure 3. Clinical Characteristics

Clinical Variable	Subtype 1	Subtype 2	Total	% of patients	Subtype 1 vs. 2, p-value
Age (Yr)					
≤60	6	5	11	68.75	0.5879
>60	4	1	5	31.25	
Sex					
Male (M)	2	3	5	31.25	0.2995
Female (F)	8	3	11	68.75	
Previously treated for NHL					
Yes	2	3	5	31.25	0.2995
No	8	3	11	68.75	
Age, Sex					
≤60, M	1	2	3	18.75	0.3882
≤60, F	5	3	8	50.00	
>60, M	1	1	2	12.50	
>60, F	3	0	3	18.75	
Age, Previously treated for NHL					
≤60, Yes	1	2	3	18.75	0.3882
≤60, No	5	3	8	50.00	
>60, Yes	1	1	2	12.50	
>60, No	3	0	3	18.75	
Sex, Previously treated for NHL					
M, Yes	1	2	3	18.75	0.5218
M, No	1	1	2	12.50	
F, Yes	1	1	2	12.50	
F, No	7	2	9	56.25	
Sex, Age, Previously treated for NHL					
M,<=60,prev Rx NHL	0	1	1	6,25	>0.99
M,<=60,not prev Rx NHL	1	1	2	12.50	
M,>60,prev Rx NHL	1	1	2	12.50	
M,>60,not prev Rx NHL	0	0	0	0	
F,<=60,prev Rx NHL	1	1	2	12.50	
F,<=60,not prev Rx NHL	4	2	6	37.50	
F,>60,prev Rx NHL	0	0	0	0	
F,>60,not prev Rx NHL	3	0	3	18.75	

Table S6, related to Figures 4 and 5. (Provided in .xls format)

Expression values for TFs with motifs located in variable DREs.

Table S7, related to Figure 6. Sanger Confirmation of SNVs

SNV position	Sample	Reference Allele	SNV	Sanger Results Tumor	Sanger Results PBMC	Variant confirmed
chr16:86028704	FL11	C	T	C/T	T	Y
chr18:60767176	FL1	C	T	C/T	C	Y
chr18:60773649	FL1	T	G	T/G	T	Y
chr1:9690142	FL5	G	C	G/C		Y
chr1:16161310	FL2	G	A	G/A		Y
chr1:146556381	FL14	T	G	T		N
chr4:774746	FL10	A	C	A/C		Y
chr5:43008282	FL2	A	G	A/G		Y
chr5:43018447	FL5	C	T	C/T		Y
chr5:132441234	FL2	A	G	G/A		Y
chr7:139875528	FL1	G	C	G		N
chr11:65190196	FL1	A	G	A/G		Y
chr11:65192186	FL10	G	A	G/A		Y
chr12:90103524	FL11	G	A	G/A		Y
chr17:1104507	FL16	C	T	C/T		Y
chr18:60768373	FL1	G	C	G		N
chr18:60768727	FL1	G	A	G		N
chr21:26940817	FL10	T	A	T/A		Y
chr21:26944186	FL10	G	C	G/C		Y
chr3:33429969	FL1	T	A	T/A	T/A	Y
chr5:42994920	FL14	C	G	C/G	C/G	Y
chr5:42994921	FL14	G	T	G/T	G/T	Y
chr5:43008176	FL14	T	C	T/C	T/C	Y
chr7:28194673	FL14	G	A	A/G	A/G	Y
chr7:130615173	FL14	T	C	T/C	T/C	Y
chr11:65185941	FL14	G	A	G/A	G/A	Y
chr11:65192335	FL14	G	A	G/A	G/A	Y
chr22:22511585	FL14	G	C	G/C	G/C	Y

Supplemental Experimental Procedures

Patient Samples. De-identified excisional lymph node biopsies were obtained from 18 patients prior to therapy (Siteman Cancer Center, WUSM) under an IRB-approved protocol with patients providing informed consent. When possible, PB samples were collected prior to treatment. All biopsies were reviewed by hematopathologists and diagnosed as FL based on morphology, immunohistochemistry, and flow cytometry. Tonsils were obtained from elective surgery (Children's Hospital, WUSM, St. Louis) in accordance with the WUSM Human Studies Committee Board. PB also was drawn from healthy volunteers by Volunteers for Health at WUSM with IRB approval.

Lymphoma Cell Lines. OCI-Ly7 (germinal center B cell-like diffuse large B cell lymphoma (GCB-DLBCL) and RL (DLBCL) were obtained from DSMZ (Braunschweig, Germany). GM12878 (lymphoblastoid B cell) was obtained from Coriell Institute for Medical Research (Camden, NJ, USA). Raji (Burkett's B cell lymphoma) was kindly provided by T. Fehniger. Cell lines were maintained in RPMI media supplemented with 10% fetal calf serum, 5 mM L-glutamine and 5 mM penicillin–streptomycin at 37°C with 5% carbon dioxide.

ChIP Assays. Cells were formaldehyde cross-linked (1% final concentration) for 10 minutes at room temperature in RPMI with 10% FBS. Crosslinking was quenched with the addition of 1M glycine (125 mM final concentration) for 5 minutes at room temperature. Cells were washed with cold PBS and lysed in an SDS buffer (1% SDS, 10 mM EDTA, 50 mM Tris [pH 8.0], dH_2O) with EDTA-free protease inhibitors (Roche, France) for 20 minutes on ice. Chromatin was fragmented using a Bioruptor (Diagenode, Denville, NJ, USA) to an average size of less

than 300 bp. Sonicated lysates were subjected to immunoprecipitation overnight at 4°C with acetylated H3 antibody (Millipore, Billerica, MA, USA), acetylated H3K27 antibody (Abcam, Cambridge, MA, USA), monomethylated H3K4 antibody (Abcam) or isotype control antibody (Santa Cruz Biotechnologies, Santa Cruz, CA, USA) conjugated to Dynabeads (Invitrogen, USA) coated with Protein-A. Samples were washed for 3 minutes at 4°C with the following buffers: low-salt buffer (0.1% SDS, 1% Triton X-100, 2 mM EDTA, 20 mM Tris [pH 8.0], 150 mM NaCl, dH_2O), high-salt buffer (0.1% SDS, 1% Triton X-100, 2 mM EDTA, 20 mM Tris [pH 8.0], 500 mM NaCl, dH_2O), LiCl buffer (0.25 M LiCl, 1% NP-40, 1% deoxycholate, 1 mM EDTA, 10 mM Tris [pH 8.0], dH_2O), and 1X Tris-EDTA buffer, and eluted with an SDS buffer (1% SDS, 0.1 M $NaHCO_3$, dH_2O). Following elution, cross-links were reversed overnight with 5 M NaCl at 65°C and immunoprecipitated DNA was isolated using spin purification columns (Qiagen, Valencia, CA, USA) as per manufacturer's instructions. At least 3 ng of ChIP, or input DNA was used for indexed library preparation. Samples were pooled and subjected to 42 bp single-end sequencing according to the manufacturer's protocol (Illumina HiSeq2000, San Diego, CA).

FAIRE. Preparation of samples for FAIRE was carried out essentially as described (Giresi and Lieb, 2009). Aliquots of five million cells were cross-linked as described for ChIP-seq. Cross-linked chromatin was lysed for 10 minutes sequentially in L1 buffer (50mM Hepes KOH pH 7.5, 140mM NaCl, 1mM EDTA pH 8.0, 10% glycerol, 5% NP40 and 0.25% Triton X-100) followed by L2 buffer (200mM NaCl, 1mM EDTA pH 8.0, 0.5mM EGTA pH 8.0, 1M and Tris pH 8.0). The pellets were resuspended in 300 µl of buffer L3 (1mM EDTA pH 8.0, 0.5mM EGTA pH 8.0, 1M Tris pH 8.0, 100mM NaCl, 0.1% Na-deoxycholate and 5mg/ml N-lauroyl sarcosine)

with EDTA-free protease inhibitors (Roche, France) and subjected to sonication using a Bioruptor (Diagenode) to an average size of 500bp. The soluble DNA fraction was isolated by performing two consecutive phenol:chloroform:isoamylalcohol (25:24:1, pH 8) extractions followed by a chloroform-isoamyl alcohol (24:1) extraction. Precipitated DNA was resuspended in 10mM Tris-HCl (pH 7.4) and incubated with 10 μg of RNase A for 1hr. Samples were then purified using spin columns (Qiagen).

Epigenome Analysis Pipeline. Sequencing tags from FAIRE- and ChIP-Seq were aligned to the reference genome (build GRCh37/hg19) with Novoalign (Hatem et al., 2013). MACS (Feng et al., 2012) was used to identify FAIRE, H3ac, H3K27ac, or H3K4me1 peaks by comparison of matched treatment to input samples using the following changes to the default settings: --nomodel --shiftsize=150 (ChIP-seq), --nomodel --shiftsize=50 (FAIRE-seq). Overlapping peaks for all chromatin marks were merged to generate a consolidated list of putative regulatory elements. Sequencing tags in 200 bp bins spanning these merged regions were pulled from wig files and reads per million (RPM) aligned reads calculated. RPM reads were then quantile normalized. Average values for control CC samples were used as the denominators to determine fold change. REs were designated as variable if their FAIRE, H3ac or H3K27ac change were two fold increased or decreased. Due to limiting cell numbers, some of the 18 FL samples did not have all assays performed; the following indicates the total FL samples with data available for each assay type. Expression microarray: 16, RNA-Seq: 10, FAIRE: 12, H3K9ac: 12, H3K27ac: 9.

Open Chromatin Clustering. DNase I-hypersensitive site (DHS) data for mammary epithelial (HMEC), embryonic stem cells (H7 and H9), T lymphocytes (TH1, TH2, TH0) and

hematopoietic progenitor ($CD34^+$) cells (Bernstein et al., 2012; Thurman et al., 2012) were downloaded from NCBI Gene Expression Omnibus (GEO, accessions GSE29692, GSE32970, and GSE18927 and subjected to MACS analysis using the previously defined FAIRE parameters. We merged overlapping peaks across all cell types using BEDTools (Quinlan and Hall, 2010) and calculated the Euclidean distance between two cell types using vectors of binary values. For each element, a cell type received a ‘‘1’’ if it contained a peak enveloped by the merged region or ‘‘0’’ otherwise. Pairwise Euclidean distances were calculated and the cell types clustered using *hclust* (nearest-neighbor algorithm) and *dendrogram* functions in the R statistical package (http://www.r-project.org).

BCL2-IgH Translocations. BCL2-IgH rearrangements were detected in FL-derived genomic DNA by Taq-man real-time PCR. Reactions contained primers and fluorescently labeled probes specific to the major breakpoint region (MBR) or minor cluster region (MCR) of the t(14;18)(q32;21) translocation. A control primer set (EEFIG) was designed to assess DNA quality.

t(14;18)(q32;q21)Translocation Primers

Primer	Sequence	Reference
MBR primer	TTAGAGAGTTGCTTTACGTGGCC	(Weinberg et al., 2007)
MBR probe^	TTTCAACACAGACCCACCCAGAGCC	
MCR primer	CCTGGCTTCCTTCCCTCTGT	(Weinberg et al., 2007)
MCR probe^	TCTCTGGGGAGGAGTGGAAAGGAAGG	
JH	GACCTGAGGAGACGGTGACC	
EEFIG Fwd	TTCAGTTTGCAAAGCTTCAGG	NA
EEFIG Rev	TACTGCATGCCAGACCCTGT	
EEF1G Probe^	TCCTCTTCTGGTCTTTGCAAAC	

^ Fluorescent internal probes labeled at the 5′ end with the reporter dye FAM and at the 3′ end with the quencher dye TAMRA

Assigning Commandeered Elements to Other Cell Types. REs present in at least one FL sample but not overlapping with normal B cell sample sets or with GM12878 ENCODE data

were assigned as *de novo*. DNase I-hypersensitive site (DHS) data for non-B cell types (Bernstein et al., 2012; Thurman et al., 2012) were downloaded from the UCSC Browser and overlapping peaks were merged using BEDTools (Quinlan and Hall, 2010). Using a binary vector, a cell type received a ‘‘1’’ if an element contained a peak enveloped by the merged region or ‘‘0’’ otherwise. The consolidated list of DHS was intersected with *de novo* REs. Normal cell types were separated from cancerous and the resultant binary matrices were used to generate heatmaps in R (http://www.r-project.org).

Gene Ontology and Pathway Analysis. Gene ontology (GO) annotation and Kyoto Encyclopedia of Genes and Genomes (KEGG) pathway analyses were performed using DAVID (Huang et al., 2009). Lists of up- or down-regulated genes (2-fold) located ±500 kb of *de novo* or attenuated REs, respectively, were generated by comparing FLs with average CC expression array data. Gene Set Enrichment Analysis (GSEA) using gene sets available from MSigDB (http://www.broadinstitute.org/gsea/msigdb/index.jsp) identified significantly enriched biological pathways (Subramanian et al., 2005).

Enriched Motif Analysis: DRE *de novo* motifs were identified using MEME version 4.9.0 in the MEME suite (Bailey et al., 2009) or RSAT (Thomas-Chollier et al., 2012). After removing repeat regions with RepeatMasker (Tempel, 2012), DNA sequences from the center of DRE FAIRE peaks were subjected to motif analysis. Sequence motifs enriched in promoters of up- or down-regulated pathway genes were identified using g:Profiler (Reimand et al., 2011)**.** Motifs were analyzed by TOMTOM in the MEME suite (Bailey et al., 2009) for comparison against

Human and Mouse (Jolma et al., 2013) and JASPAR (Portales-Casamar et al., 2010) databases of known transcription factor motifs.

Cloning for Luciferase Assays. DREs were amplified and, with the exception of DRE8, inserted into Bam HI and Sal I sites downstream of the luciferase coding sequence in the SV40 promoter-driven pGL3 plasmid (Promega). DRE8 was blunted into the enhancer position of pGL3 plasmid. Mutations corresponding to the relevant SNVs were introduced into the luciferase vectors using Q5 site-directed mutagenesis (New England Biolabs, IPswich, MA, USA).

Luciferase assay cloning primers

Primer Name	Sequences
IgH Enhancer Fwd	GGATCCCGGCCCCGATGCGGGACTGCG
IgH Enhancer Rev	GACGGCCACTCTATCAGAATATC
DRE1 Fwd	GGATCCCCCGGTCTTAACTGTTTCTATATGT
DRE1 Rev	GTCGACTCCGCAAAGCTCAGTCATGT
DRE2 Fwd	GGATCCCCCCCGTTCCCTGTGAGTTA
DRE2 Rev	GTCGACCATGGAGACCTCACCGCAG
DRE3 Fwd	GGATCCTGTCTTCCTCTTCCCTGCTT
DRE3 Rev	GTCGACTACCAACCTCCCTGCAAAGT
DRE4 Fwd	GGATCCTCTCCACCCTGTCTTCCCAT
DRE4 Rev	GTCGACCAGCAGTGAGTTCCTCAGGG
DRE5 Fwd	GGATCCCTGCCATCCTCTCTTGCCTC
DRE5 Rev	GTCGACGGGAGTCCCATGCCATCTTC
DRE6 Fwd	GGATCCAGGATCTATCTCATCGGGGCA
DRE6 Rev	GTCGACCCAACACATGCTCGACCTTT
DRE7 Fwd	GGATCCTAGCCAGAGCAGACCAGCTA
DRE7 Rev	GTCGACCCCCAAGAGGGCTGTGAAAT
DRE8 Fwd	GGATCCTTCCCCAGGTCAAGTCCTCT
DRE8 Rev	GTCGACTGTGGGATTGTGTACGCATGT
DRE9 Fwd	GGATCCTCTTCCATGCCAAGCTCAG
DRE9 Rev	GTCGACTCCCTGGACTGAAGTCCTCT
DRE10 Fwd	GGATCCGGCTTGACTGCTGACTCCTT
DRE10 Rev	GACTTATTCATGGCATGGGCAGC
DRE15 Fwd	CCCCGGATCCTGTGAAGCAGAGTAAAGACTGAGA
DRE15 Rev	CCCCGTCGACCCTGGGCTTTGAATTTAGGCAG
DRE16 Fwd	CCCCGGATCCCTTTTCTCCACACCCACACG
DRE16 Rev	CCCCGTCGACGCCTTAATCTGTCCTCGCCA
DRE17 Fwd	CCCAGGATCCGCACAGCGGAACCAGGTA
DRE17 Rev	CCCCGTCGACCATGAATGAGAAGCGAGACCC

Enrichment of SNPs in variable DREs. GWAS SNPs associated with neonatal diseases, immune disease, nervous system disease, body measurements, non-B cell cancers, inflammatory disease, cardiovascular disease, and behavior and addiction were downloaded from NCBI's debags database (http://www.ncbi.nlm.nih.gov/projects/gapplusprev/sgap_plus.htm) in April 2014. SNPs not located on the main chromosome contigs, SNPs without a dbSNP ID and SNP records that contained multiple SNPs associated with a particular trait were excluded from analysis. Enrichment of trait-associated SNPs was calculated as the proportion of SNPs associated with a given trait in variable DREs divided by the proportion of all SNPs in variable DREs (p). Significance of the enrichment was calculated as previously described (Maurano et al., 2012) using the binomial equation with x being equal to the number of SNPs associated with a given trait, n equal to the total number of SNPs associated with that trait and p to the previously calculated value.

Oligonucleotide Precipitation Assays

Biotinylated complementary oligonucleotides were annealed and incubated with whole cell lysates from 293T cells transfected with 5 μg of CMV promoter driven TCF3, IKZF1, or SP1 expression plasmid using TransIT (Mirus, Madison, WI, USA) transfection reagent.

OPA oligonucleotides

Name	Sequences
Ikaros reference	TGACGCTGGATTCTCCCTGCTAGTGATGCA
Ikaros variant	TGACGCTGGATTCTCTCTGCTAGTGATGCA
SP1 reference	CAGGAGGGAGCGGCGGGGGAGGAGGGGGTG
SP1 variant	CAGGAGGGAGCGGCGAGGGAGGAGGGGGTG
TCF3 reference	AGATCGAGGTGCCAGCTGCTAAGAGGGGTC
TCF3 variant	AGATCGAGGTGCCAGTTGCTAAGAGGGGTC

Analysis of knockdown experiments. Cells transfected with control or SPIB shRNA were purified by CD4 selection 48 hours post transfection. The abundance of mRNA transcripts was assessed by quantitative PCR. To assess the impact on DRE activity, purified cells were subjected to H3K27ac ChIP assay and quantitative PCR.

Realtime oligonucleotides

Name	Assay	Sequences	Source
CABLES1 sense	RT-PCR	GGACGGAGGAAGACAATCAA	(Park et al., 2007)
CABLES1 antisense	RT-PCR	CAGGTTACGGAACTGGGAGA	
COL4A2 sense	RT-PCR	GAAGTTTGATGTGCCGTGTGG	(Fuchshofer et al., 2007)
COL4A2 antisense	RT-PCR	CTTTACGTCCCTGCAGCCC3	
DUSP10 sense	RT-PCR	AAGAGGCTTTTGAGTTCATTGAG	(Leyva-Illades et al., 2010)
DUSP10 antisense	RT-PCR	CAAGTAAGCGATGACGATGG	
GAPDH sense	RT-PCR	ATGGGGAAGGTGAAGGTCG	
GAPDH antisense	RT-PCR	GGGTCATTGATGGCAACAATATC	
RAB20 sense	RT-PCR	CCCAAGGGCACCTAAGCA	(Wang et al., 2005)
RAB20 antisense	RT-PCR	CCAGCATCTTGTACTTGAGGATCTT	
SPIB sense	RT-PCR	GGGCCACACTTCAGCTGTCT	(Talby et al., 2006)
SPIB antisense	RT-PCR	CAGTCCAGTCCCACAGGGAG	
TET2 sense	RT-PCR	TTCGCAGAAGCAGCAGTGAAGAG	(Liu et al., 2013)
TET2 antisense	RT-PCR	AGCCAGAGACAGCGGGATTCCTT	
TMEM241 sense	RT-PCR	GGTCTCTGGTCGGCCTCACCTT	(Hansen et al., 2012)
TMEM241 antisense	RT-PCR	TGAGCGTCTGCCACCCTTGGA	
DRE11 sense	ChIP	CCCAGGCAGTGATGGCTTTA	
DRE11 antisense	ChIP	AGGCTCGGCACTCCTATGTA	
DRE12 sense	ChIP	GACCAGTTCTGTGGGTAGGG	
DRE12 antisense	ChIP	CAGTGGATTGTCCAAGCGTC	
DRE13 sense	ChIP	GCCTTACCTTGGACCCTTACC	
DRE13 antisense	ChIP	GGAACCTCGGATGGCACTTT	
DRE14 sense	ChIP	GACTTCTGGGAGGAACAGCC	
DRE14 antisense	ChIP	GTGGTTGCACAGGTAGTGGA	

Statistical Analyses. Comparison of expression of all genes near variable DREs or genes with concordant changes in TSS chromatin was performed by unpaired t-test with Welch's correction. Comparison of expression for selected genes in samples with or without variable DREs was performed using the Mann-Whitney test. The significance of SNV and SNP enrichment in variable DREs was calculated by χ^2 test. The significance of variable DREs enrichment in conventional enhancer was calculated by Fisher's exact test.

Supplemental References

Bailey, T.L., Boden, M., Buske, F.A., Frith, M., Grant, C.E., Clementi, L., Ren, J., Li, W.W., and Noble, W.S. (2009). MEME SUITE: tools for motif discovery and searching. Nucleic Acids Res. *37*, W202–8.

Bernstein, B.E., Birney, E., Dunham, I., Green, E.D., Gunter, C., and Snyder, M. (2012). An integrated encyclopedia of DNA elements in the human genome. Nature *489*, 57–74.

Dave, S.S., Wright, G., Tan, B., Rosenwald, A., Gascoyne, R.D., Chan, W.C., Fisher, R.I., Braziel, R.M., Rimsza, L.M., Grogan, T.M., et al. (2004). Prediction of survival in follicular lymphoma based on molecular features of tumor-infiltrating immune cells. N. Engl. J. Med. *351*, 2159–2169.

Feng, J., Liu, T., Qin, B., Zhang, Y., and Liu, X.S. (2012). Identifying ChIP-seq enrichment using MACS. Nat. Protoc. *7*, 1728–1740.

Fuchshofer, R., Yu, A.H.L., Welge-Lüssen, U., and Tamm, E.R. (2007). Bone morphogenetic protein-7 is an antagonist of transforming growth factor-beta2 in human trabecular meshwork cells. Invest. Ophthalmol. Vis. Sci. *48*, 715–726.

Giresi, P.G., and Lieb, J.D. (2009). Isolation of active regulatory elements from eukaryotic chromatin using FAIRE (Formaldehyde Assisted Isolation of Regulatory Elements). Methods *48*, 233–239.

Hansen, H.G., Schmidt, J.D., Søltoft, C.L., Ramming, T., Geertz-Hansen, H.M., Christensen, B., Sørensen, E.S., Juncker, A.S., Appenzeller-Herzog, C., and Ellgaard, L. (2012). Hyperactivity of the Ero1α oxidase elicits endoplasmic reticulum stress but no broad antioxidant response. J. Biol. Chem. *287*, 39513–39523.

Hatem, A., Bozdağ, D., Toland, A.E., and Catalyürek, U. V (2013). Benchmarking short sequence mapping tools. BMC Bioinformatics *14*, 184.

Huang, D.W., Sherman, B.T., and Lempicki, R.A. (2009). Systematic and integrative analysis of large gene lists using DAVID bioinformatics resources. Nat. Protoc. *4*, 44–57.

Jolma, A., Yan, J., Whitington, T., Toivonen, J., Nitta, K.R., Rastas, P., Morgunova, E., Enge, M., Taipale, M., Wei, G., et al. (2013). DNA-binding specificities of human transcription factors. Cell *152*, 327–339.

Leich, E., Salaverria, I., Bea, S., Zettl, A., Wright, G., Moreno, V., Gascoyne, R.D., Chan, W.-C., Braziel, R.M., Rimsza, L.M., et al. (2009). Follicular lymphomas with and without translocation t(14;18) differ in gene expression profiles and genetic alterations. Blood *114*, 826–834.

Leyva-Illades, D., Cherla, R.P., Galindo, C.L., Chopra, A.K., and Tesh, V.L. (2010). Global transcriptional response of macrophage-like THP-1 cells to Shiga toxin type 1. Infect. Immun. *78*, 2454–2465.

Liu, R., Jin, Y., Tang, W.H., Qin, L., Zhang, X., Tellides, G., Hwa, J., Yu, J., and Martin, K.A. (2013). Ten-eleven translocation-2 (TET2) is a master regulator of smooth muscle cell plasticity. Circulation *128*, 2047–2057.

Maurano, M.T., Humbert, R., Rynes, E., Thurman, R.E., Haugen, E., Wang, H., Reynolds, A.P., Sandstrom, R., Qu, H., Brody, J., et al. (2012). Systematic localization of common disease-associated variation in regulatory DNA. Science *337*, 1190–1195.

Neph, S., Vierstra, J., Stergachis, A.B., Reynolds, A.P., Haugen, E., Vernot, B., Thurman, R.E., John, S., Sandstrom, R., Johnson, A.K., et al. (2012). An expansive human regulatory lexicon encoded in transcription factor footprints. Nature *489*, 83–90.

Park, D.Y., Sakamoto, H., Kirley, S.D., Ogino, S., Kawasaki, T., Kwon, E., Mino-Kenudson, M., Lauwers, G.Y., Chung, D.C., Rueda, B.R., et al. (2007). The Cables gene on chromosome 18q is silenced by promoter hypermethylation and allelic loss in human colorectal cancer. Am. J. Pathol. *171*, 1509–1519.

Portales-Casamar, E., Thongjuea, S., Kwon, A.T., Arenillas, D., Zhao, X., Valen, E., Yusuf, D., Lenhard, B., Wasserman, W.W., and Sandelin, A. (2010). JASPAR 2010: the greatly expanded open-access database of transcription factor binding profiles. Nucleic Acids Res. *38*, D105–10.

Quinlan, A.R., and Hall, I.M. (2010). BEDTools: a flexible suite of utilities for comparing genomic features. Bioinformatics *26*, 841–842.

Reimand, J., Arak, T., and Vilo, J. (2011). g:Profiler--a web server for functional interpretation of gene lists (2011 update). Nucleic Acids Res. *39*, W307–15.

Subramanian, A., Tamayo, P., Mootha, V.K., Mukherjee, S., Ebert, B.L., Gillette, M.A., Paulovich, A., Pomeroy, S.L., Golub, T.R., Lander, E.S., et al. (2005). Gene set enrichment analysis: a knowledge-based approach for interpreting genome-wide expression profiles. Proc. Natl. Acad. Sci. U. S. A. *102*, 15545–15550.

Talby, L., Chambost, H., Roubaud, M.-C., N'Guyen, C., Milili, M., Loriod, B., Fossat, C., Picard, C., Gabert, J., Chiappetta, P., et al. (2006). The chemosensitivity to therapy of childhood early B acute lymphoblastic leukemia could be determined by the combined expression of CD34, SPI-B and BCR genes. Leuk. Res. *30*, 665–676.

Tempel, S. (2012). Using and understanding RepeatMasker. Methods Mol. Biol. *859*, 29–51.

Thomas-Chollier, M., Darbo, E., Herrmann, C., Defrance, M., Thieffry, D., and van Helden, J. (2012). A complete workflow for the analysis of full-size ChIP-seq (and similar) data sets using peak-motifs. Nat. Protoc. *7*, 1551–1568.

Thurman, R.E., Rynes, E., Humbert, R., Vierstra, J., Maurano, M.T., Haugen, E., Sheffield, N.C., Stergachis, A.B., Wang, H., Vernot, B., et al. (2012). The accessible chromatin landscape of the human genome. Nature *489*, 75–82.

Victora, G.D., Dominguez-Sola, D., Holmes, A.B., Deroubaix, S., Dalla-Favera, R., and Nussenzweig, M.C. (2012). Identification of human germinal center light and dark zone cells and their relationship to human B-cell lymphomas. Blood *120*, 2240–2248.

Wang, V., Davis, D.A., Haque, M., Huang, L.E., and Yarchoan, R. (2005). Differential gene up-regulation by hypoxia-inducible factor-1alpha and hypoxia-inducible factor-2alpha in HEK293T cells. Cancer Res. *65*, 3299–3306.

Weinberg, O.K., Ai, W.Z., Mariappan, M.R., Shum, C., Levy, R., and Arber, D.A. (2007). Minor'' BCL2 breakpoints in follicular lymphoma: frequency and correlation with grade and disease presentation in 236 cases. J. Mol. Diagn. *9*, 530–537.